Nov 7th, 12:00 AM - Nov 8th, 12:00 AM

A Preliminary Study on Stainless Steel Hollow Flange Beams Featuring Lateral-Distortional Buckling

Shuang Niu

Zhidong Zhang

Feng Fan

Wei-Wen Yu International Specialty Conference on Cold-Formed Steel Structures
St. Louis, Missouri, U.S.A., November 7 & 8, 2018

A Preliminary Study on Stainless Steel Hollow Flange Beams Featuring Lateral-Distortional Buckling

Shuang NIU [1], Zhidong ZHANG [2], Feng FAN [3]

Abstract

To explore the potential of using stainless steel structurally, extensive research has been carried out to study the structural behavior of stainless steel member as associated with the nonlinear stress-strain relationship. Hollow flange sections feature improved structural efficiency and a unique issue of web distortion. Steel hollow flange sections have been studied and commercially distributed (e.g. the very first HFB section and lately LSB section). As a proactive study, this paper investigates stainless steel hollow flange beams of double-symmetric section with numerical modeling and parametric analysis. The validity of the idealized FE model was verified with existing study on steel counterparts. Specifically, three alloys (S30401, S44330, S32101) and a series of sections and member

[1] Assistant Professor, School of Civil Engineering, Harbin Institute of Technology, Harbin 150090, PR China. <aniu216@126.com>

[2] Ph.D. student, Department of Civil Engineering, Johns Hopkins University, Baltimore, MD 21218, USA. <zhidongzhang@jhu.edu>

[3] Professor, School of Civil Engineering, Harbin Institute of Technology, Harbin 150090, PR China. < fanf@hit.edu.cn >

spans were covered. Preliminary conclusions were drawn about the effects of material nonlinearity, work-hardening and lateral-distortional buckling on the member strengths. Performance of current design provisions (AS4100, AS/NZS4600, EC3, CECS410) were evaluated and it was found that Eurocode 3-1.4 beam design curve has a better overall prediction of the member strength.

Introduction

Hollow flange beams comprise an innovative type of cold-formed sections (see Fig. 1). They offer structural efficiency mainly due to the torsionally rigid closed flanges refraining the member flexural-torsional buckling and the flange local buckling. Strength enhancement in material is also obtained in the cold-worked flanges. However, because of the relatively slender web element, hollow flange beams are affected by lateral-torsional buckling, featuring simultaneous lateral deflection, twist, and web distortion. Two types of steel hollow flange beams (Fig. 1) have ever been extensively studied and commercially distributed under the name HFB (Hollow Flange Beam) and LSB (Lite-Steel Beam developed by LiteSteel Technologies) respectively. Note that 'HFB' in this context refers to the beam with a section of Fig. 1(a). While stainless steel HFBs are not yet seen in practical use, they offer an attractive structural solution and might be used to further explore the benefits in structural application of stainless steel.

(a) HFB section. (b) LSB section.

Fig. 1 Two hollow flange sections in practical use.

Cross-sections

The HFB sections in Avery(2000) were adopted for the current study and the precise dimensions are tabulated in Table 1. '45090HFB38' in Avery(2000) or '450-38' for abbreviation both denote the cross-section of 450mm height (external size) and 3.8mm thickness, all sections' b taken as 74mm.

Table 1. Dimensions (mid-plane size) of HFBs for FE modeling in current study (units: mm)

Designation		H	h	b	r	t	b/t	h/t
45090HFB38	450-38	446.2	370	74	6.1	3.8	19.5	97.4
40090HFB38	400-38	396.2	320	74	6.1	3.8	19.5	84.2
35090HFB38	350-38	346.2	270	74	6.1	3.8	19.5	71.1
30090HFB38	300-38	296.2	220	74	6.1	3.8	19.5	57.9
30090HFB33	300-33	296.7	219	74	6.35	3.3	22.4	66.4
30090HFB28	300-28	297.2	218	74	6.6	2.8	26.4	77.9
25090HFB28	250-28	247.2	168	74	6.6	2.8	26.4	60.0
25090HFB23	250-23	247.7	168	74	6.85	2.3	32.2	73.0
20090HFB23	200-23	197.7	118	74	6.85	2.3	32.2	51.3

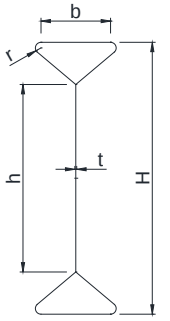

Numerical model and calibration

Numerical models were developed with software package ABAQUS 6.11. For loading and boundary conditions, pinned ends and uniform bending moment were modeled without introduction of warping constraints. A scheme shown in Fig. 2 was used. Three reference points RP1~RP3 were first created at both member ends, then a rigid body constraint was imposed taking RP1 as the active node and the RP2, RP3 and web edge as slave parts. Another two sets of multipoint constraints (MPC) were then defined over the two hollow flanges taking RP2 and RP3 as the active nodes and the hollow flange edges as the slave parts. End restraints and bending moments were applied at the controlling node

“RP1” at both ends. Specifically, at one end Ux、Uy、Uz、URx were restrained, and at the other end Uy、Uz、URx were restrained (longitudinal direction x and vertical direction y).

For material properties, Austenitic S30401, ferritic S44330, and lean duplex S32101 as per the ASTM unified numbering system were considered and they are also simply referred to as 304, 443 and 2101 in this paper. The cold-forming process of HFB sections result in considerable strength enhancement in the entire hollow flange region, a schematic figure of nominal strength within a HFB section is provided in Fig. 3, in which the web region assumes virgin sheet material properties and the hollow flange (flange flat portions and corners) assumes higher strengths. It is also necessary to distinguish the compression and tension part of the section. These strengths were evaluated with the related literature including Cruise&Gardner (2008), Ashraf&Gardner (2005), Huang&Young (2012), Niu (2014), Rasmussen (2003). And in order to eliminate the stress concentration caused by concentrated bending moment at both FE model ends, the material was set to be ideal elastic in the 20 mm spans at both ends. The virgin flat material properties of three alloys are available in Niu(2014), and tensile material parameters in the current study are listed in Table 2. The engineering stress-strain relationships above are also transformed into true stress-strain relationships as inputs of ABAQUS.

Table 2. Engineering material parameters in tension used in the current study

Material		Austenitic S30401 (304)			Ferritic S44330 (443)			Lean duplex S32101 (2101)		
		Web	Flange	Corner	Web	Flange	Corner	Web	Flange	Corner
E_0	(GPa)	198.1	198.1	195.6	201.5	201.5	209.3	198.2	198.2	205.5
n	(\)	6.5	6.5	4.7	13.1	13.1	6.2	6.9	6.9	4.5
$f_{0.2}$	(MPa)	244.9	415	700	287.9	488	536	489.8	830	757.7
f_u	(MPa)	719.7	844	1543	428.3	524	568	709.3	852	890

The consistent mode imperfection was incorporated into the FE model based on the ABAQUS BUCKLE analysis. The lowest order lateral-torsional buckling

mode and local buckling mode were first normalized. And according to Avery (2000), the lateral-torsional buckling mode imperfection amplitude is taken as Length/1000 while local buckling mode imperfection amplitudes of the flange and the web are taken as 0.01*B and d/150 respectively where B denotes total flange width and d represents net web height.

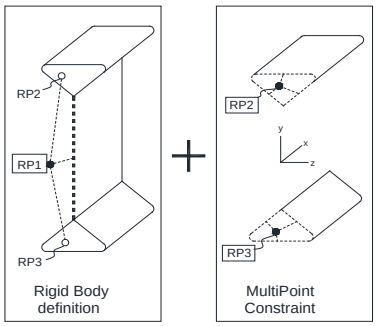

Fig. 2 Pinned end connection modeling.

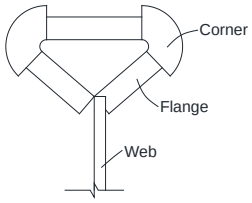

Fig. 3 Nominal strengths within a HFB section.

Cold working process would bring about the nonlinear residual stress distribution including the membrane and bending components. Jandera &Gardner (2008) and Gardner&Cruise (2009) show that the membrane stress value is relatively low while the bending stress value is relatively high which could make a difference in the member structural performance. The material parameters adopted in current study were from the tests whose coupons were cut from the raw steel plate in Niu(2014). Referenced from Jandera &Gardner (2008), the bending residual stress component's distribution law of a quadrate section is indicated in Fig. 4 and the distribution law along the thickness direction is presented in Fig. 5. The bending residual stress amplitude of the corner portion is $0.37*\sigma_{0.2}$ while the flat portion amplitude is $0.63*\sigma_{0.2}$. The ABAQUS SIGINI subroutine was adopted to incorporate the bending residual stress in the FE model.

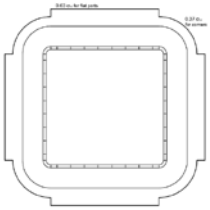

Fig. 4 Bending residual stress distribution law in the quadrate steel section.

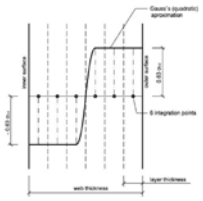

Fig. 5 Bending residual stress distribution law along the thickness direction.

Shell element S4R was adopted for the FE model. Mesh sizes of 30mm, 20mm, 10mm were adopted to generate different FE models for convergence check. The results show that 20mm mesh size could guarantee the simulation convergence and accuracy, also improving the computational efficiency.

Due to vacancy of experimental data of stainless steel HFBs, results for its steel counterparts in Avery (2000) were used for calibration of idealized FE models. So the HFB idealized FE model's material properties, member imperfections and residual stresses were defined the same as the corresponding settings in Avery (2000). Taking 450-38 and 250-23 section for validity check, the validity check results are close, and only the 450-38 section check results are presented in Table 3. The elastic buckling critical load and the nonlinear ultimate capacity are listed in column (1) and (4) while the corresponding values in Avery (2000) are listed in column (2) and (5), respectively. The ratios of this paper's value to Avery's value are listed in column (3) and (6), respectively. It could be found that the current FE model's prediction values are very close to those of Avery (2000) model which were verified against experiment data. Therefore, the current model is deemed accurate enough and it is modified in material constitutive behaviors to investigate their stainless steel counterparts.

Table 3. 45090HFB38 model validity check results

Span(m)	(1) (kN.m)	(2) (kN.m)	(3)(%)	(4) (kN.m)	(5) (kN.m)	(6)(%)
1.5	197.55	194.80	1.01	142.39	141.15	1.01
2.0	126.24	125.60	1.01	105.87	107.39	0.99
2.5	94.82	94.90	1.00	84.58	86.77	0.97
3.0	78.21	78.50	1.00	72.12	74.17	0.97
4.0	60.81	60.90	1.00	58.06	58.58	0.99
5.0	51.01	50.80	1.00	49.71	49.64	1.00
6.0	44.21	43.80	1.01	43.71	43.29	1.01
8.0	34.98	34.20	1.02	35.55	34.62	1.03
		Average	1.01		Average	1.00
		SD	0.007		SD	0.019

Parametric study and results

Parametric study was carried out to reveal the effects of material nonlinearity, cold-work hardening, and lateral-distortional buckling on the member strength. Three scenarios of material model were proposed.

Model A: As shown in Fig. 6(a), The web is assigned with the virgin flat sheet material properties. The stainless steel sheet is first roll-formed into a closed circular section and then roll-formed into a triangle hollow flange, so the flange flat portion adopts enhanced material properties and the flange corner area adopts higher strength material properties. According to Cruise&Gardner (2008), four portions with 2*t width neighbouring the two flange corners should be assigned with material properties same with the flange corners where t is the section thickness.

Model B: As indicated in Fig. 6(b), both the web and the flange flat portion are assigned with the virgin flat sheet material properties. Only the flange corner is assigned with enhanced material properties because it will not buckle and its strength is always effective. So this scenario is calculated as a conservative lower bound of the member capacity, following the same principle of current

stainless steel design standards (i.e. no strength enhancement due to cold-forming is included in the member strength indices).

Model C: A hypothetical material called 304E with the same nominal strength of 304 stainless steel and an ideal bi-linear stress strain relationship, is further introduced into the model B. Other settings of model C are the same with model B. Through the comparison between B and C models, a better understanding of stainless steel nonlinearity effects on member performance could be obtained.

To sum up, model A harnesses strength enhancements while model B does not account for the strength enhancements of flange flat portion. And model C adopts artificial 304E material (bilinear stress-strain curves) for appreciating the effects of gradual yielding and strain hardening on the member strength.

(a) Model A. (b) Model B.

Fig. 6 Two nominal strength assignment schemes within a HFB section.

In this paper, 470 specimens were simulated in total, covering nine cross-sections, ten spans ranging from 0.25m to 10m, four material properties including 304, 443, 2101 stainless steel and artificial 304E material, and two material assignment schemes.

After conducting the *elastic buckling analysis* of each case, it could be seen that three most common buckling modes are global-distortional buckling, web and flange local buckling (see Fig. 7). Local buckling of webs and flanges tended to be low order buckling modes in short span members while global-distortional buckling tended to be the leading mode in medium and long span members.

After conducting the *nonlinear analysis* of each case, it could be found that many cases with a span not less than 2m tend to have a lateral-distortional

buckling failure mode, so HFB section stainless steel beams are significantly affected by the web distortion in addition to the lateral buckling.

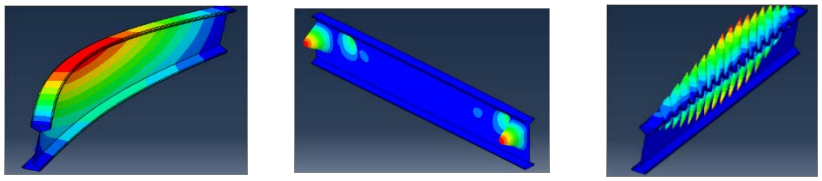

Global-distortional buckling Local buckling of webs Local buckling of flanges

Fig. 7 Representative overall and cross-section views of three most common buckling modes.

The member stress distribution state at peak moment was investigated. Taking the 300-33 section 304 stainless steel B material assignment scheme cases as an example, Fig. 8 presents the MISES stress distribution of four members of different spans. The colorized portion's stress is higher than the proof yield stress $f_{0.2}$ at failure moment while the white portion's stress is lower than $f_{0.2}$. As the member span decreases, the section strain development level gradually increases and the white portion area gradually decreases. So short span members' capacity tend to be controlled by material strength and local buckling while long span members' capacity tend to be controlled by global buckling.

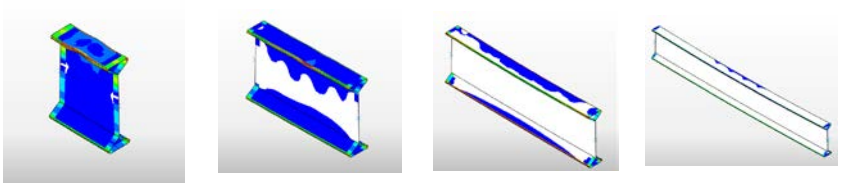

(a) 0.25m (b) 0.5m (c) 1m (d) 2m

Fig. 8 Stress distribution of 300-33 section 304 stainless steel B material assignment scheme members at failure moment.

Current study incorporated a hypothetical material 304E to investigate the effects of material nonlinearity on the member strength. The nonlinear ultimate capacity analysis of the 450-38, 350-38, 300-33, 250-28, and 200-23 section HFBs with 304E material (material assignment scheme C) and different spans were carried out. And the results were compared with those counterparts of material assignment scheme B, as presented in Fig. 9. The member span is taken

as the abscissa while the member capacity M_u normalized by section first yield moment M_y is taken as the ordinate. M_u/M_y values of 304 stainless steel members are larger than the corresponding 304E members in the short span cases (not larger than 1m) while in the medium and long span cases (larger than 2m) M_u/M_y values of 304 stainless steel members are lower than 304E members. The plasticity of short span members tends to develop well and the strain hardening of stainless steel is more obvious, so the material nonlinearity has favorable effects on member capacity (member capacity tends to be close to the section capacity). The medium and long span members tend to be controlled by global-distortional buckling and the failure stress level is lower than the proof yield stress, so the decrease in the elastic modulus caused by gradual yielding leads to the member strength reduction.

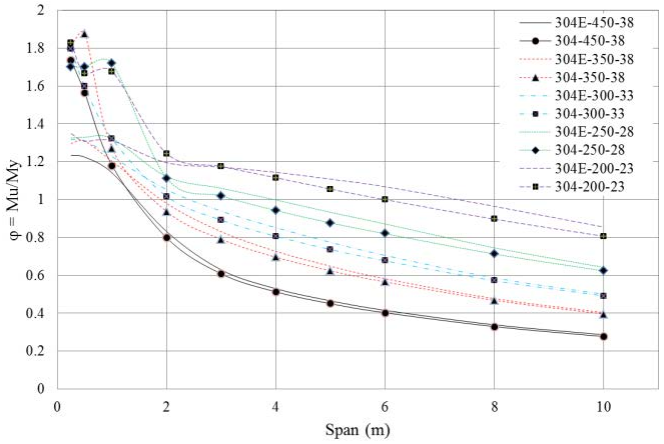

Fig. 9 Comparison of ultimate bearing capacity of B and C material model HFBs with different sections and different spans.

Performance of current Design standards

The parametric analysis result data were processed using two parameters, one is the coefficient φ as defined in the Eqn(1a), and the other one is the normalized

section slenderness ratio λ as defined in the Eqn(1c). In Eqn(1a), M_u is the member ultimate capacity while M_y (indicated in Eqn(1b)) is the nominal first yield moment defined by gross section modulus W (also expressed as Z_g) and the proof yield strength of the virgin material $f_{0.2}$. In Eqn(1c), normalized slenderness ratio λ is defined using M_y and the elastic buckling critical moment M_{cr}. For the conventional I section beams, M_{cr} tends to be defined as the elastic global buckling critical load M_o (see Eqn(1d)). And based on the previous discussion, the HFBs tend to be affected by lateral-distortional buckling. Referenced from Trahair (1997) and Bradford (1992), the elastic global-distortional buckling critical load M_{od} is adopted as M_{cr} (see Eqn (1e)). BUCKLE analysis based on refined FE model was used to get M_{od} and formulas from Trahair (1997) (see Eqn (3)) was used to solve for M_{od} when it is difficult to obtain it with BUCKLE analysis (for example the very short span members which tend to be dominated by various localized buckling modes).

$$\varphi = \frac{M_u}{M_y} = \frac{M_u}{W \cdot f_{0.2}} \quad \text{Eqn(1a)}$$

$$M_y = W \cdot f_{0.2} \quad \text{Eqn(1b)}$$

$$\lambda = \sqrt{\frac{M_y}{M_{cr}}} \quad \text{Eqn(1c)}$$

$$\lambda = \sqrt{\frac{M_y}{M_o}} \quad \text{Eqn(1d)}$$

$$\lambda = \sqrt{\frac{M_y}{M_{cr}}} = \sqrt{\frac{W \cdot f_{0.2}}{M_{od}}} \quad \text{Eqn(1e)}$$

Referenced from related standards and literature, six bending design curves incorporating the normalized slenderness ratio λ are presented as following: (1) the Australian steel structures standard AS4100 (1998) design curve (see Eqn(2)); (2) Trahair (1997) proposed a modified design curve for the steel HFBs based on the former curve (see Eqn(3)); (3) the design curve of the European steel structures design code Eurocode3-1.1 (2005)(see Eqn(4a)) and the parameter φ_e is got from Eqn(4b); (4) The European stainless steel structures design code Eurocode 3-1.4 design curve (1996)(see Eqn(4a)) and the parameter φ_e is shown in Eqn(4c); (5) China's technical stainless steel structures design specification CECS 410's design curve (2015)(see Eqn(4a) and Eqn(4d)). The

design curve of Australian cold-formed steel structures standard AS4600 (2005)(see Eqn (5)).

$$\varphi = 0.6(\sqrt{\lambda^4 + 3} - \lambda^2) \quad \text{Eqn(2)} \qquad \phi_e = 0.5\left[1 + 0.34(\lambda - 0.4) + \lambda^2\right] \quad \text{Eqn(4c)}$$

$$\varphi = 0.6(\sqrt{\lambda^4 + 2.8} - \lambda^2) \quad \text{Eqn(3)} \qquad \phi_e = 0.5\left[1 + 0.65(\lambda - 0.41) + \lambda^2\right] \quad \text{Eqn(4d)}$$

$$\varphi = \frac{1}{\phi_e + \sqrt{\phi_e^2 - \lambda^2}} \quad \text{Eqn (4a)}$$

$$\phi_e = 0.5\left[1 + 0.34(\lambda - 0.2) + \lambda^2\right] \quad \text{Eqn (4b)}$$

$$\varphi = \begin{cases} 1 & \lambda \le 0.6 \\ 1.11\left[1 - (\lambda^2/3.6)\right] & 0.6 < \lambda < 1.336 \\ 1/\lambda^2 & \lambda \ge 1.336 \end{cases} \quad \text{Eqn(5)}$$

All the processed strength data points (420 in total) and six related bending strength design curves are plotted in Fig. 10. In this figure's legend, 'A-304' indicates simulations adopting 304 stainless steel and material assignment scheme A; 'AS4100-carbon steel' stands for Australian steel structures standard AS4100 design curve; 'Trahair-carbon steel' represents the modified design curve for the steel HFBs proposed by Trahair (1997); 'Eurocode3-carbon steel' stands for the design curve of the European steel structures design code curve; 'Eurocode3-Stainless steel' represents the European stainless steel structures design code curve; 'AS4600-cold formed steel' represents the Australian cold-formed steel structures standard AS4600 design curve; 'CECS410-stainless steel' stands for the China's technical stainless steel structures design specification CECS410 design curve.

For members in small slenderness range (limiting slenderness locates approximately at λ=0.7 for material Model B, and λ=0.8 for material Model A), φ factors greater than 1.0 are found demonstrating that the strengths were controlled by section capacity. Another phenomenon worth noting is that material assignment scheme B members' strength are lower than those scheme A counterparts at all slenderness range, demonstrating flange flat portion's strength enhancements (cold-work hardening effects) makes a considerable contribution to the member capacity, which becomes increasingly significant as

member slenderness decreases.

Comparing the strength data points with design curves, it was found 'AS4600-cold formed steel' curve predicts not conservative strength for nearly all members with intermediate to high slenderness, though for small slenderness members its predictions become conservative. All the other design curves lie below the collection of data points, with 'Eurocode3-Stainless steel' curve giving the best predictions. Actually, 'Eurocode3-Stainless steel' curve is still quite conservative as compared with the collection of strength data. It's approximately equal to or slightly lower than the lower bound line of the collection of data in most part of the slender range.

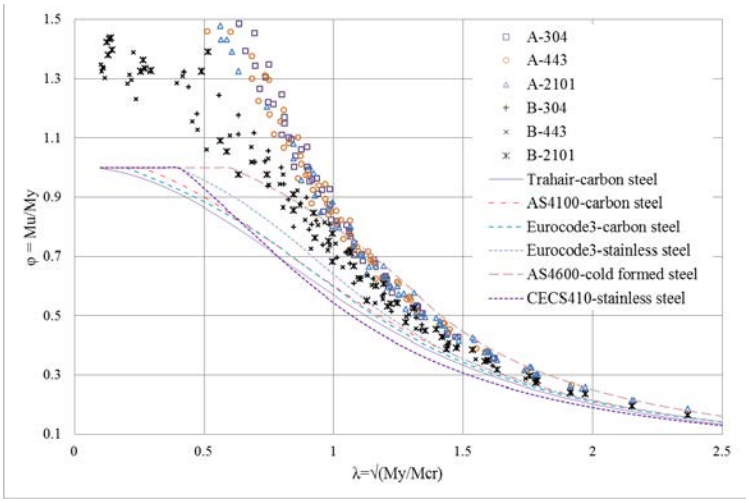

Fig. 10 Comparison of stainless steel HFB parametric analysis strength data points and six related design curves.

Conclusions

(1) HFB section features strong flanges with a slender web, and therefore it is significantly affected by the web distortion in addition to the lateral buckling. So the lateral-distortional buckling critical load M_{od} obtained with numerical

methods or formulas should be taken as M_{cr} for use in relevant bearing capacity design curves for stainless steel HFB members.

(2) The strength enhancements of flange flat portion (cold-work hardening effects) contribute significantly to the member's ultimate bearing capacity.

(3) The material nonlinearity (strain hardening) has favorable effects on the ultimate bearing capacity M_u of short span (less than 1m) HFBs while it (gradual yielding) has negative effects on M_u of medium and long span (larger than 2m) HFBs because of the different stress levels at failure.

(4) Material assignment scheme B in the current study conservatively applies the virgin material properties without considering flange flat portion strength enhancements, which is in line with the principle of current stainless steel standards adopting minimum nominal properties. The resulting member strength from scheme B is therefore considerably lower than those of material assignment scheme A, which considers the flange flat portion strength enhancements. Eurocode3-1.4 design curve were found predicting quite conservative strength even for material assignment scheme B results.

References

Ashraf, M., Gardner, L., & Nethercot, D. A. (2005). Strength enhancement of the corner regions of stainless steel cross-sections. Journal of Constructional Steel Research, 61(1), 37-52.

Australia Standards (AS). (1998). Steel structures, AS 4100:1998, Sydney, Australia.

Avery, P., Mahendran, M., & Nasir, A. (2000). Flexural capacity of hollow flange beams. Journal of Constructional Steel Research, 53(2), 201-223.

Bradford, M. A. (1992). Lateral-Distortional buckling of steel I—Section members. Journal of Constructional Steel Research, 23(1-3), 97-116.

Cruise, R. B., & Gardner, L. (2008). Residual stress analysis of structural stainless steel sections. Journal of Constructional Steel Research, 64(3), 352-366.

Cruise, R. B., & Gardner, L. (2008). Strength enhancements induced during cold forming of stainless steel sections. Journal of Constructional Steel Research, 64(11), 1310-1316.

EN 1993-1-1. (2005). Eurocode 3: design of steel structures - part 1-1: general rules and rules for buildings.

ENV 1993-1-4. (1996). Eurocode 3: design of steel structures - part 1-4: supplementary rules for stainless steel.

Gardner, L., & Cruise, R. B. (2009). Modeling of residual stresses in structural stainless steel sections. Journal of Structural Engineering, 135(1), 42-53.

Huang, Y., & Young, B. (2012). Material properties of cold-formed lean duplex stainless steel sections. Thin-walled structures, 54, 72-81.

Jandera, M., Gardner, L., & Machacek, J. (2008). Residual stresses in cold-rolled stainless steel hollow sections. Journal of Constructional Steel Research, 64(11), 1255-1263.

Niu, S. (2014). Interaction Buckling of Cold-Formed Stainless Steel Beams. The University of Sydney, Harbin Institute of Technology: Australia, China.

Pi, Y. L., & Trahair, N. S. (1997). Lateral-distortional buckling of hollow flange beams. Journal of Structural Engineering, 123(6), 695-702.

Rasmussen, K. J. (2003). Full-range stress–strain curves for stainless steel alloys. Journal of constructional steel research, 59(1), 47-61.

Standards Australia. (2005). Cold-formed steel structures. AS/NZS4600-2005, Sydney, Australia

Standards China. (2015). Technical specification for stainless steel structures. CECS 410-2015, Beijing (in Chinese)